energies

MDPI

Article

Characterization of Aerodynamics of Small Wind Turbine Blade for Enhanced Performance and Low Cost of Energy

Hailay Kiros Kelele [1,2,*], Lars Frøyd [3], Mulu Bayray Kahsay [2] and Torbjørn Kristian Nielsen [1]

[1] Department of Energy and Process Engineering, Norwegian University of Science and Technology, 7491 Trondheim, Norway
[2] School of Mechanical and Industrial Engineering, Mekelle University, Mekelle P.O. Box 231, Ethiopia
[3] 4Subsea AS, Hagaløkkveien 26, 1383 Asker, Norway
* Correspondence: hailay.k.kelele@ntnu.no or hailaykk@gmail.com or hailay.kiros@mu.edu.et

Abstract: During a turbine's lifetime, minimizing the cost of power production should be the primary aim in addition to attaining high technical efficiency. Thus, this paper was aimed at enhancing the aerodynamic efficiency of a site-specific small wind turbine considering the cost of energy as one of the design parameters. The wind distribution of a specific site was employed to characterize the wind using the Weibull distribution method. The aerodynamics of a typical 5 kW wind turbine blade were investigated by implementing a blade element method (BEM) using a MATLAB code that applied the advancements and improvements with different modifications and which was validated by engaging computational fluid dynamics (Ansys-Fluent). The optimal pitch angle was then employed to further promote the performance characteristics of the blade. The cost of energy was reformulated in terms of rated power considering a cost variation of the main components that deviates with the rated power. Accordingly, the performance parameters were investigated against a varying rated power and the relative cost of energy, achieving a maximum power coefficient of 55.37% at a lower cost of energy. Moreover, annual energy production of approximately 18 MWh with a corresponding capacity factor of approximately 41% was achieved at a lower cost of energy. These findings demonstrate that the selected modelling, analysis procedures, and modifications enhance the aerodynamic performance characteristics and lower the cost of energy of the small wind turbine blade, which promotes the affordability and energy harnessing capability of small wind turbines.

Keywords: aerodynamics; small wind turbine; cost of energy; blade performance characteristics; blade element method; annual energy production; capacity factor

Citation: Kelele, H.K.; Frøyd, L.; Kahsay, M.B.; Nielsen, T.K. Characterization of Aerodynamics of Small Wind Turbine Blade for Enhanced Performance and Low Cost of Energy. *Energies* **2022**, *15*, 8111. https://doi.org/10.3390/en15218111

Academic Editor: Davide Astolfi

Received: 26 September 2022
Accepted: 26 October 2022
Published: 31 October 2022

1. Introduction

Small wind turbines (SWT) receive less attention than their larger counterparts, which might be the reason leading to their low technology development. The small number of certified SWT evidences this case [1] and might contribute to a lack of confidence in the technology towards their intended use of demand. Regardless of this, the SWT global market is predicted to increase every year [2] and the scarce high potential wind resource area requirement of the large-scale wind turbines lets researchers look for an alternative in areas of lower wind potential and lower technology demanding small wind turbines [3].

Most of the earlier research focused on structural analysis rather than aerodynamic optimization. Power coefficients of approximately 25% and 45%, and a capacity factor of 20–40% and 35–45% are depicted for the small- and large-scale wind turbines, respectively [4–6]. Advances in aerodynamic performance and optimization of turbines with the readily available broad application airfoils, which can be used for small wind turbine applications, would create dramatic developments in the small wind turbine sector [4,7–10]. For example, Delft University, the Technical University of Denmark, and the National Renewable Energy Laboratory (NREL) developed several families of airfoils for wind turbine blades. Among the different airfoils available, some provided good performance characteristics in the fluid flow best suited to small-scale wind turbines [8,11,12].

The theory of the ideal design based on the Betz limit is a starting point for a realistic wind turbine blade design [13,14]. According to the Betz limit, the ideal efficiency of the wind turbine is approximately 59.3%, with an ideal value of the induction factors and corresponding chord lengths. Different adaptations are required, as the ideal design has the massive size of the blade towards the root, where its contribution in creating the torque is the least. Among the commonly practiced adaptations, simplifying the root part by drawing a straight line through the 70% and 90% span points simplifies and removes a lot of material close to the root [14]. It is shown that even though the drag will increase due to the simplified design at the modified region, the penalty due to small values of the adverse torque in that region is negligible. Moreover, modification of the ideal design is possible by simplifying the chord and twist distributions using linearization [15], implementing a simple control method via modification control points on the rotor geometry of the ideal design [16]. Furthermore, the tip loss factor is a correction for the induction factors developed using actuator disk theory, which assumes an infinite number of blades. In practice, a finite number of blades are used, which leads to the vortex structure change in the wake of the turbine [17]. Thus, Prandtl initially defined the tip loss factor, which was latter modified by Glauert [18]. In recent times, Shen further improved it and developed a modified tip loss correction model for aerodynamic computations of wind turbines, which better predicts the aerodynamic force distribution in the vicinity of the tip [19], with the improvement confirmed compared to Glauert's tip loss correction in [20]. Hence, implementing these changes with improved tip and root part modifications will help realize a better wind turbine design.

Another condition that needs due care in wind turbine aerodynamics is parameter selection. The best design parameters should be selected and implemented to maximize the performance of the wind turbine. Primarily, the number of blades and tip speed ratio requires careful nomination. Qualitative comparisons of the power coefficient versus tip speed ratio for a different number of blades are discussed in [14,21]. Furthermore, the choice of the design wind speed is another main parameter that requires careful attention. There are various commonly used ways of design/rated wind speed selection resulting in different values. The IEC-61400-2 standard is one of the most commonly used for analysis based on wind class [22] and recommends that the rated wind speed is 40% higher than the mean wind speed. On the other hand, as a rule of thumb, it is suggested that the rated wind speed is a factor of 1.5 greater than the site mean wind speed [23,24]. However, based on wind distribution characteristics, selecting the design wind speed at approximately the highest wind power distribution is expected to extract the maximum power [25].

Blade element method (BEM) and computational fluid dynamics (CFD) are widely used numerical analysis tools for the performance prediction of the wind turbines. BEM helps in determining the axial forces and torque using the linear momentum theory, while CFD helps in the visualization of flow behavior on the blade surface and the wake region [26]. BEM is the most frequently used method for aerodynamic and aero-elastic analysis. In the design of wind turbine blades, different modifications and improvements have been made for better evaluation of forces and velocities. Among these, the adjustments made in [26] indicated performance improvement at the inboard and outboard parts of the turbine. This has the advantage of reducing the flap bending moment to some extent, taking into account wake expansion and rotation [27]. In solving the flow fields using the CFD, the two-equation turbulent models of the k-ω and k-ε series and four-equation transition k-ω SST (shear stress transport) turbulent models are commonly implemented to study the Reynolds-averaged Navier–Stokes (RANS) equation. The k-ω turbulence model is appropriate in modeling the boundary layers, whereas the k-ε turbulence model is suitable for far-field flow simulations. The transition k-ω SST turbulence model has primarily been used for the aerodynamic investigation of 3D wind turbine blades implementing the k-ε model for far-field flows and k-ω model for boundary layers [28–30].

Wind turbines that support variable-speed operation utilize pitch control techniques to achieve desired power outputs. Pitch control is mainly applied in regulating the pitch angle of wind turbine blades to retain the rated power output for wind speeds above the rated values [31]. The performance of small wind turbines might be significantly improved through more effective power regulations implementing advanced pitch-to-feather control strategies [32]. The effect of pitch angle on the performance of a wind turbine was studied in [33], correlating the power produced to the stall characteristics. The effect of variable blade pitch on the aerodynamic performance of a small turbine emphasizing the enhanced behavior due to the use of a pitch angle controller is also presented in [34]. Thus, pitching is mainly used in controlling different characteristics of wind turbine operations. Additionally, attention should be given in using it for correcting twist angle to maximize the aerodynamic efficiency of wind turbines at the design phase.

On the other hand, a wind turbine is capital intensive with approximately 50% of its cost of energy related to the turbine cost [35]. Performance improvement without considering the cost of energy (CoE) might lead to limited use of small wind turbines if the power gained could not cover the associated cost of power production during the turbine's lifetime. The cost of energy is commonly assessed for wind turbines in operation at individual or wind farm levels [35,36] or used to select existing turbines based on specific site conditions, including in [37] where the site-specific wind turbine selection method is presented in terms of the radius of the rotor, hub height, and rated power as variables, assuming a cost-of-energy model. On the other hand, another study designated a minimum cost of energy as the better metric in examining common objectives used in wind turbine optimization problems [38]. Hence, it is important to consider the cost of energy as a design parameter during the design phase. In a previous study by the authors [39], the site-specific design of a blade was considered for a SWT. A detail analysis of wind resource data at four sites was employed to determine the rated power of a turbine to provide the lowest cost of energy at each site. The same blade design and hub height were assumed for the SWT for the four sites. Based on average wind speed and the estimated AEP at each site, the respective rated power at minimum cost of energy was determined.

This current paper presents design processes for a small wind turbine blade that enhances the aerodynamic performance characteristics at a reduced cost of energy considering low-to-medium, site-specific wind conditions. It employs the blade element method applying the advancements and improvements with different modifications that are not commonly implemented for small wind turbines. Moreover, the cost of energy was considered as a design parameter, redefining it in terms of rated power to enable designing low-cost-of-energy blade aerodynamics, which is not commonly considered in small wind turbine designs. Lastly, different performance measures, including the power coefficient, annual energy production, and capacity factor, were assessed against a varying rated power and the relative cost of energy attaining an enhanced performance characteristics at a minimum cost of energy. The results demonstrate designing high performance and cost-effective small wind turbines.

2. Materials and Methods

2.1. Defining Blade Design Parameters

Based on wind potential records at a height of 30 m above ground level for sites around Mekelle, located at a latitude of 13.48° N, a longitude of 39.49° E and an elevation of approximately 2200 m above sea level, the wind and power density distributions of four sites shown in Figure 1, which were evaluated using bins and statistical methods [13,40], were used for the analysis. Thus, using the method of bins for wind records classified into N_b bins, the total number of data N and average speed $\overline{V}$ of the wind were defined as:

$$N = \sum\nolimits_i^{N_b} f_i, \ \ \overline{V} = \frac{1}{N} \sum\nolimits_{i=1}^{N_b} v_i f_i \tag{1}$$

where f_i is the frequency of occurrence in each bin and v_i is the midpoint wind speed.

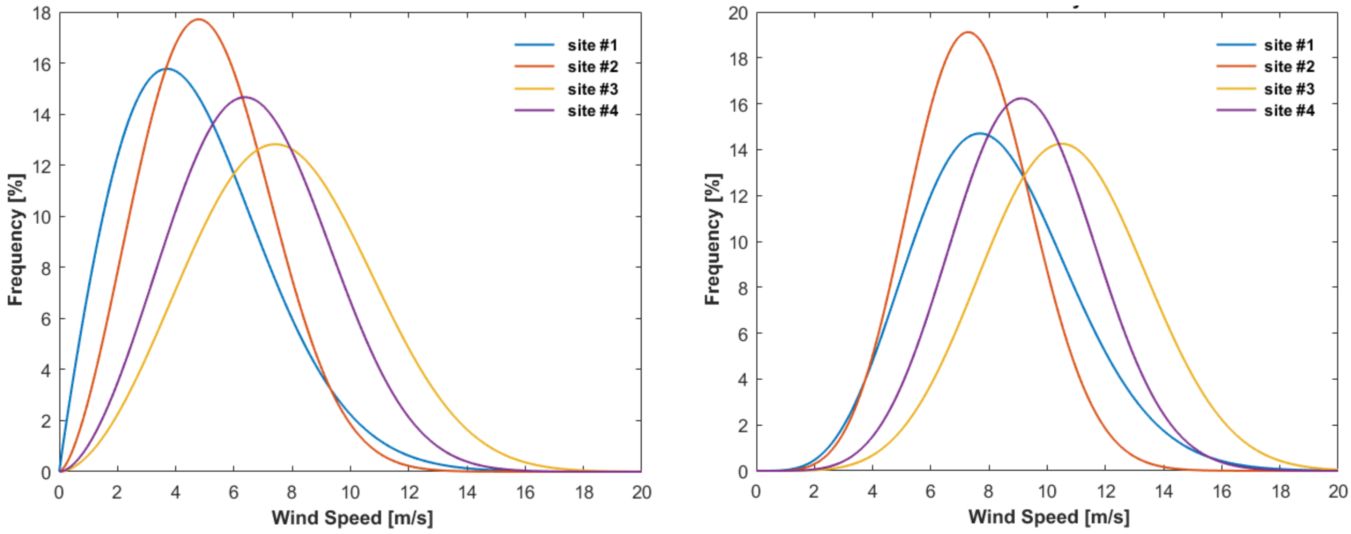

(**a**) (**b**)

Figure 1. Weibull probability distribution of low-to-medium wind characteristics of four sites around Mekelle. (**a**) Wind speed distribution. (**b**) Wind power density distribution.

The standard deviation σ_V of the wind was then calculated from:

$$\sigma_V = \sqrt{\frac{1}{N-1}\left\{\sum_{i=1}^{N_b} v_i^2 f_i - N\overline{V}^2\right\}} \tag{2}$$

Among existing probability distributions to represent wind behavior, the Weibull distribution is the most appropriate because it incorporates both the exponential and Rayleigh distributions and provides a good normal distribution approximation [13,40]. Hence, the Weibull probability density function $f(V)$ and the cumulative distribution function $F(V)$ were found from:

$$f(V) = (k/c)(V/c)^{k-1}exp\left[-(V/c)^k\right],\ F(V) = 1 - exp\left[-(V/c)^k\right] \tag{3}$$

representing the shape factor c and the shape parameter k, for $1 \leq k < 10$, as:

$$c = \overline{V}/\Gamma(1+1/k),\ k = \left(\sigma_V/\overline{V}\right)^{-1.086} \tag{4}$$

where $\Gamma(1 + {}^1/_k)$ is the gamma function defined as $\Gamma(1 + {}^1/_k) = \int_0^\infty e^{-t} t^{(1+{}^1/_k)-1} dt$.

The average power density $\overline{P}/A$ and average machine power $\overline{P}_w$ can then be evaluated as:

$$\overline{P}/A = \frac{1}{2}\rho\frac{1}{N}\sum_{i=1}^{N_b} v_i^3 f_i,\ \overline{P}_w = \frac{1}{N}\sum_{i=1}^{N_b} P_w(v_i) f_i \tag{5}$$

where A is the swept area of the rotor, ρ is the density of air, and $P_w(v_i)$ is the power produced defined by the power curve of the rotor.

The annual energy production AEP of the rotor and the capacity factor CF were also represented as:

$$AEP = E_w = \sum_{i=1}^{N_b} P_w(v_i) f_i \Delta t,\ CF = \overline{P}_w/P_r \tag{6}$$

where Δt is the time of operation in a year and P_r is rated power.

The average representative wind parameter of the four sites was then calculated based on the weighted average using the power density per unit area of each site as a weighting factor W_j, defined as:

$$W_j = \left(\overline{P}/A\right)_j / \sum_{j=1}^{n}\left(\overline{P}/A\right)_j, \quad j = 1, 2, 3 \ldots n \tag{7}$$

where n represents the number of data sites under consideration. The required parameter was evaluated as the sum of the parameters of each site multiplied by their corresponding weighting factor W_j. Accordingly, the representative weighted wind distribution, power density distribution, and cumulative distribution were evaluated, as shown in Figure 2, and were then used to design and evaluate the performance of the rotor blade.

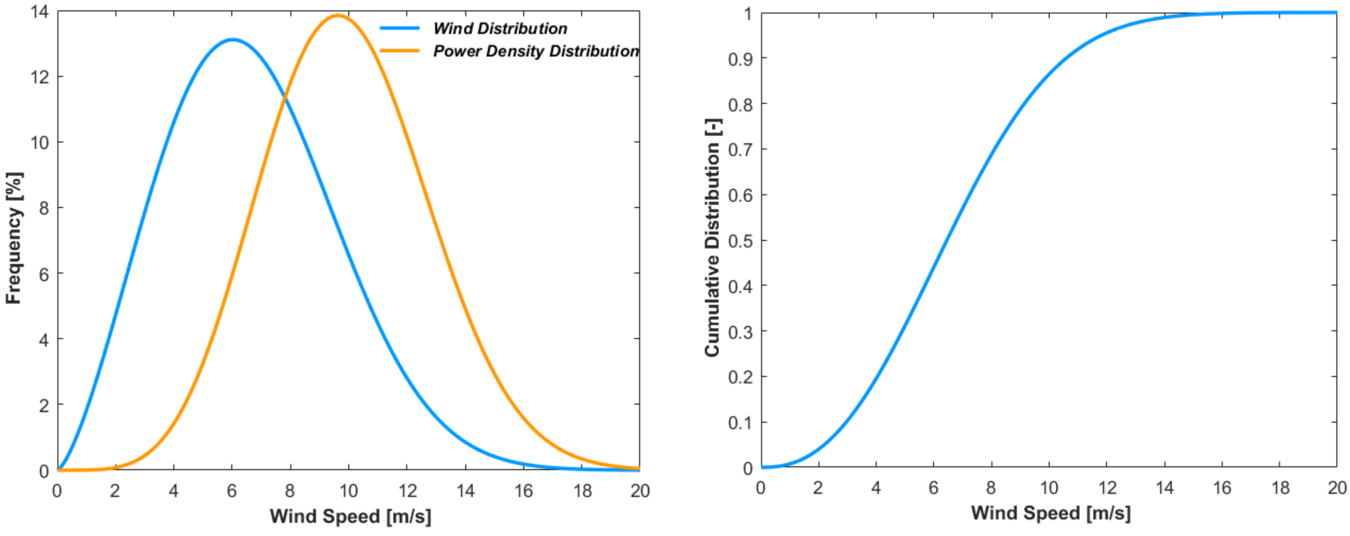

(**a**) (**b**)

Figure 2. Weighted average wind characteristics of four sites around Mekelle based on the Weibull probability distribution with k = 2.42, c = 7.51, and standard deviation SD = 2.95. (**a**) Frequency distribution. (**b**) Cumulative distribution.

To maximize the performance of the rotor, the selection of best design parameters plays a vital role. The tip speed ratio, number of blades, and design wind speed are the most influential parameters in designing aerodynamically efficient wind turbines. Therefore, a tip speed ratio (*TSR* or λ) of 7 with a three-bladed horizontal-axis wind turbine is the most efficient combination, as per the qualitative comparisons in power coefficients for rotors of different configurations [14,21]. Designing for specific wind characteristics, wind speed around the highest wind power distribution is expected to extract maximum wind power [25]. Hence, according to the power density distribution shown in Figure 2, selecting a design wind speed in the range of 8–12 m/sec would be advantageous. This would be confirmed by varying the design wind speed according to the performance parameters and cost of energy. Zero pitch angle was also taken during the initial design phase, which is subject to change after considering its effect.

In addition to these criteria, environmental conditions such as density ρ and the kinematic viscosity ν of air affect the design of wind turbines. These values were taken based on the elevation and atmospheric pressure of the selected area. The design parameters used are shown in Table 1.

Table 1. Design parameters and values.

Atmospheric Parameters and Values	*Blade Parameters and Values*
Density of air, $\rho = 0.92$ (kg/m^3)	Power, $P_d = 5$ (kW)
Viscosity of Air, $\nu = 1.87 \times 10^{-5}$ (m^2/s)	Tip Speed Ratio, TSR or $\lambda = 7$ (-)
Atmospheric Pressure = 780 (hPa)	Number of Blades, $N_{Bl} = 3$ (-)
Design Wind Speed, $V_0 = 8$–12 (m/s)	Pitch Angle = 0°

Small wind turbines commonly use one airfoil throughout the blade length, which contributes to their low performance compared to their larger counterparts. Hence, mixed airfoils were proposed to improve the performance as airfoils have maximum lift-to-drag coefficient ratios at a specific thickness. Thicker airfoils are required around the root to withstand the higher moments, while thin airfoils are required around the tip of the blade to enhance aerodynamic lift forces. Thus, it is better to use different airfoils at different radial positions according to their thickness variation in the rotor. Accordingly, the S823 and S822 set of airfoils of the NREL, developed for small wind turbines (1–5 m long and 2–20 kW) and having good performance for rough leading edges [9,10], were selected. A rectangular section was selected as a third airfoil for use in the root part to properly connect the blade with the hub plate.

Their corresponding lift coefficient C_l and drag coefficient C_d were used at a specific angle of attack α for S822 and S823 and the recommended force coefficient by IEC 61400-2 [22] was selected for the rectangular section. According to their aerodynamic behavior and thickness, the above airfoils were then arranged along the blade span. Moreover, their corresponding slopes were evaluated at the selected angle of attack α from C_l and C_d data around the linear region. Hence, Table 2 shows the airfoils used and their corresponding parameters. Hybrid airfoils were used employing interpolations for radial positions out of the specified spans. Similarly, the aerodynamic coefficients of the hybrid airfoils were determined using interpolation based on their radial locations and thicknesses. Figure 3 shows the sample arrangements of the airfoils and the interpolated ones at their respective radial positions.

Table 2. Aerodynamic parameters of the selected airfoils.

Parameter/Airfoil	*S822*	*S823*	*Rectangular*
Airfoil thickness (m)	*0.16*	*0.26*	*0.30*
Lift coefficient, C_l (-)	*0.7936*	*0.8388*	*0*
Drag coefficient, C_d (-)	*0.00678*	*0.0157*	*1.5*
Angle of attack, A (°)	*4.75*	*6.25*	*0*
Slope (-)	*6.2*	*6.5*	*0*

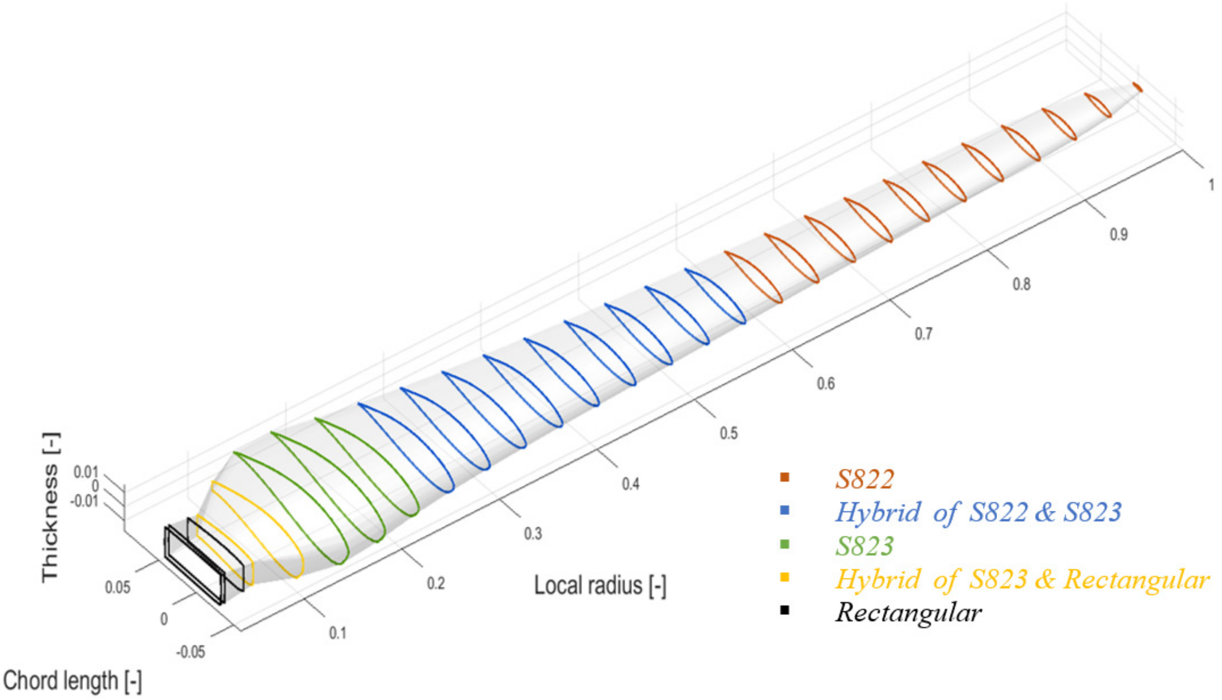

Figure 3. Sample arrangement of the different airfoils along the span of the blade.

2.2. Creating Universal Blade Parameter

The ideal design method based on the Betz limit was used to initiate the design of the blade. It was defined based on the following relationship, assuming negligible effects of the drag force as an initial design. Hence, the local speed ratio λ_r is related to axial induction factor a and tangential induction factor a' as:

$$\lambda_r = (4a-1)\sqrt{1-a/1-3a}\,,\quad a' = 1-3a/4a-1 \tag{8}$$

where r is a radial position along the blade span.

The ideal twist angle β is defined in terms of the flow angle φ and design angle of attack α_d as:

$$\beta = \varphi - \alpha_d,\ \varphi = tan^{-1}\left[(1-a)V_0/(1+a')\omega r\right] \tag{9}$$

where ω is angular rotor speed and V_0 is the wind speed.

The chord length L_c and the blade design parameter B_{ep} were then defined as:

$$B_{ep} = 4asin\varphi/(1+a') \tag{10}$$

$$L_c = B_{ep}\left[2\pi V_0/N_{Bl}C_{l,d}\omega\right] = 8\pi aV_0 sin\varphi/(1+a')N_{Bl}C_{l,d}\omega \tag{11}$$

where N_{Bl} is the number of blades and $C_{l,d}$ is the design lift coefficient at the design angle of attack α_d.

Thus, the universal blade parameter B_{ep} was found, given the above ideal relationship at the ideal values of $a = 1/3$ and $a' = 0$ or close to zero. Once this blade parameter was found, it was used as a universal value for the rest of the blade design, unless the initial input design values P_d, $C_{l,d}$, N_{Bl}, α_d, V_0, and λ were changed. At this stage, the ideal blade geometry, in terms of the ideal chord lengths and ideal twist angles, was ready for further realistic modifications. This ideal design of the blade was then used as an input to the design modifications with all the input parameters described above.

2.3. Implementation of the Blade Element Method

The definitions of the *BEM* were according to the explanations in [26,27]. Hence, the axial and tangential aerodynamic forces were expressed in terms of their corresponding coefficients, the axial or normal force coefficient C_n, and tangential or rotational force coefficient C_r as:

$$C_n = C_l cos\varphi + C_d sin\varphi,\ C_r = C_l sin\varphi - C_d cos\varphi \tag{12}$$

The thrust and torque coefficients C_T and C_Q, respectively, were expressed as:

$$C_T = V_{rel}^2 C_n L_c N_{Bl}/2\pi r V_0^2 = \sigma\, C_n V_{rel}^2/V_0^2 \tag{13}$$

$$C_Q = V_{rel}^2 C_r L_c N_{Bl}/2\pi r V_0^2 = \sigma\, C_r V_{rel}^2/V_0^2 = C_T\left(C_r/C_n\right) \tag{14}$$

where V_{rel} is the relative wind velocity, as shown in Figure 4, which illustrates the relationships between the aerodynamic forces, velocities, twist, and attack angles. The solidity factor σ was defined as:

$$\sigma = L_c N_{Bl}/2\pi r \tag{15}$$

The axial induction factor for $a < 0.2$, can be expressed as:

$$a = \left[\left(8\pi r F sin^2\varphi/C_r L_c N_{Bl}\right) + 1\right]^{-1} \tag{16}$$

where F is the tip loss factor. Otherwise, the polynomial relationship developed in [26] was implemented as:

$$a = k_1\left(C_T/F\right) + k_2\left(C_T/F\right)^2 + k_3\left(C_T/F\right)^3 \tag{17}$$

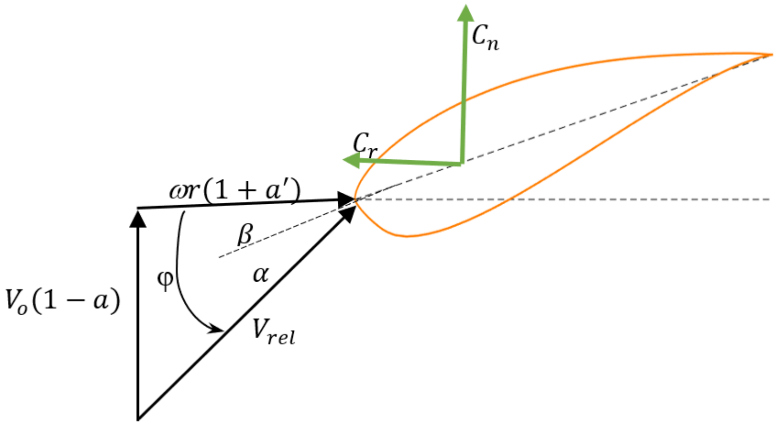

Figure 4. Representation and relationships of aerodynamic forces, velocities, and angles.

This empirical relationship was developed for unconed and undeflected rotors, with the coefficients k_i determined from numerical actuator disk analysis as $k_1 = 0.08921$, $k_2 = 0.05450$, and $k_3 = 0.25116$ [26]. The tangential induction factor a', which is the same for all conditions, was expressed as:

$$a' = {}^{C_Q}/_{4(1-a)\lambda_r} \tag{18}$$

where $\lambda_r = {}^{\omega r}/_{V_0}$.

The Shen tip loss factor, which is the modified version of Glauert's tip loss correction factor, developed to correct the assumption of an infinite number of blades, was selected as it better predicts the aerodynamic force distribution in the vicinity of the tip [19,20] and was described as:

$$F = \frac{2}{\pi} cos^{-1}\left(e^{-g\frac{N_{Bl}}{2}\left(\frac{R-r}{rsin\varphi}\right)}\right) \tag{19}$$

where g is the addition by Shen and is expressed as $g = exp[-0.125(N_{Bl}\lambda_r - 21)] + 0.1$.

2.4. Chord Modifications

Prior to applying the BEM, the Shen tip loss factor was applied for the chord modification around the blade tip. Moreover, chord modification methods discussed in [15,16] were included. The control points around the root and the maximum chord were increased. In addition, more control points were utilized around the starting point of the modified region, taking the starting point of the chord modification at approximately 60% of the blade span, as shown in Figure 5. These were applied in MATLAB code in such a way, selecting the stated control points, that a smooth profile was generated employing Bezier curve principles facilitating smooth connections between the ideal and modified points of the root and the hub. It was also used to control or limit the maximum chord value.

The remaining span beyond 60% was taken from the ideal value to maximize the energy harnessing ability and the performance of the wind turbine blade. Element-wise, this part of the blade span contributes most of the energy compared to the others. However, the tip loss correction factor was applied to this part to correct the losses. Figure 5 shows the ideal and modified blade chord, including the control points for modification around the root, mid, and tip of the blade spans.

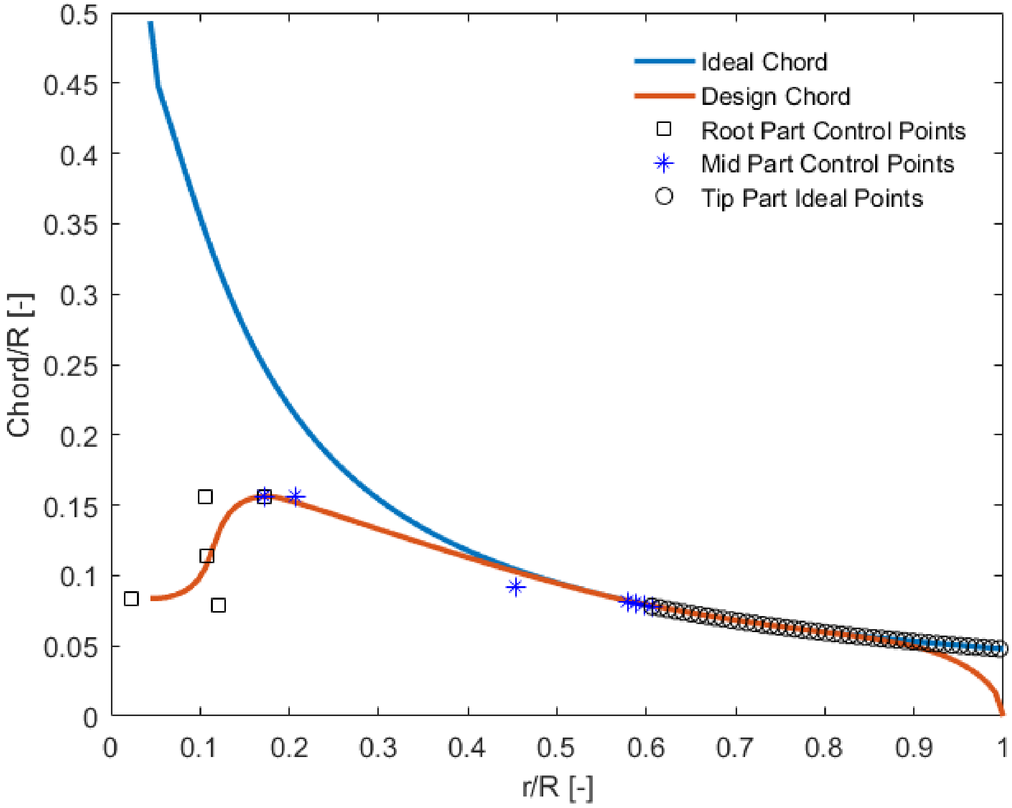

Figure 5. Modification of the ideal chord implementing a smooth curve using control points and a Bezier curve.

2.5. Twist Modifications

Affected by the modifications of the blade, the chord length was made to be less than the ideal one, starting at approximately 60% of the span towards the root of the rotor. Hence, the ideal angle of attack α_d in the modified part results in lower aerodynamic torque due to deviation of the axial induction factor from the ideal value. Therefore, the twist angle β was modified by increasing α_d to compensate for the axial induction factor. Even though this modification will increase the C_d, the effect is less than the associated increase of C_l [14]. The twist angle modification was assumed to be within the linear range of the C_l versus α curve, considering the operating conditions would not exceed this region. Accordingly, the twist modification was defined as outlined below.

The normal force coefficient $C_{n,\ new}$ that would compensate for the deviation of the ideal induction factor [16] was described as:

$$C_{n,new} = 4Fsin^2\varphi/\sigma\left(\frac{1}{a_d} - 1\right) \tag{20}$$

With the assumption that the change in C_l is more than the change in C_d in the linear region, the modified lift coefficient was then defined as:

$$C_{l,new} = (C_{n,new} - C_d sin\varphi)/cos\varphi \tag{21}$$

For the linear region change in the angle of attack, α was described as:

$$\Delta\alpha = \Delta C_l/(\partial C_l/\partial\alpha) = C_{l,new} - C_l/(\partial C_l/\partial\alpha) \tag{22}$$

The corrected twist angle β_{new} applied in the iterative loop was then defined as:

$$\beta_{new} = \varphi - (\alpha_d + \Delta\alpha) \tag{23}$$

2.6. Power and Force Evaluation

After implementing the above modifications in Sections 2.4 and 2.5, the local rotor thrust force dT and torque dQ were evaluated as:

$$dT = \frac{1}{2} N_B L_c C_n \rho \frac{V^2 (1-a)^2}{\sin^2 \varphi} dr,\ dQ = \frac{1}{2} N_B L_c C_r \rho \frac{V(1-a)}{\sin \varphi} \frac{r\omega (1+a')}{\cos \varphi} dr \tag{24}$$

The total thrust force T, torque Q, and rotor shaft power P_{rotor} were defined as:

$$T = \int_{R_{hub}}^{R} dTdr = \sum_{i=1}^{N_{el}} dT_i \Delta r,\ Q = \int_{R_{hub}}^{R} dQrdr = \sum_{i=1}^{N_{el}} r_i dQ_i \Delta r,\ P_{rotor} = Q\omega \tag{25}$$

The shaft power coefficient C_p and the thrust force coefficient C_t were also represented as:

$$C_p = {}^{Q\omega}/_{\frac{1}{2}\rho V_0^3 A}\ ,\ C_t = {}^{T}/_{\frac{1}{2}\rho V_0^2 A} \tag{26}$$

where A is the swept area of the rotor.

Hence, a new value of radius R_{new} was defined, given the above expressions and the design power P_d, to update the radius in the iterative loop as:

$$R_{new} = R\sqrt{P_d / Q\omega} \tag{27}$$

The angular speed of the rotor, which was updated in the iteration in terms of R_{new}, was then defined as:

$$\omega\ = \lambda V_0 / R_{new} \tag{28}$$

2.7. Cost of Energy and Performance Characteristics

Specific wind characteristics represented by the Weibull wind distribution, power density distribution, and cumulative distributions shown in Figure 2 were considered to evaluate the performance parameters of the designed blade. The annual energy production AEP, capacity factor CF, and rated wind speed V_r were analyzed against the rated power P_r variation. Besides enhancing the technical efficiency, minimizing the cost of power production should be given priority. Hence, the cost of energy CoE, which represents the production cost of unit energy [13], was represented as:

$$CoE = [C_{ce} \times FCR + C_{om}] / AEP \tag{29}$$

where C_{ce} is the wind turbine capital cost, FCR is a fixed charge rate, and C_{om} is the operations and maintenance costs. With a limited scope of study about the cost impacts, CoE was analyzed in terms of the rated power using cost elements changing with rated power variation. Thus, the cost of power electronics and the drive train were anticipated to vary proportional to the rated power, while the cost of the blade was assumed to vary with the square root of the rated power [23]. The drive train cost component should be ignored for direct-drive small wind turbines.

Thus, the turbine capital cost C_{ce} was proposed to be defined as a function of the rated power based on the cost variation of the main components that deviate with the rated power as:

$$C_{ce} = \left(C_{Bl} \times \sqrt{P_r} + (C_{pe} + C_{dt}) \times P_r + C_{oc} \right) \tag{30}$$

where C_{Bl} is cost of the blade, C_{pe} is the cost of power electronics, C_{dt} is the cost of the drive train, and C_{oc} is other component costs.

Therefore, the CoE was reformulated up on the proposed relationship of the turbine capital cost in Equation (30), as:

$$CoE = \left[\left(C_{Bl} \times \sqrt{P_r} + (C_{pe} + C_{dt}) \times P_r + C_{oc} \right) \times FCR + C_{om} \right] / AEP \tag{31}$$

To evaluate the *CoE*, component level contributions for land-based turbines according to the NREL [35] were converted into percent contributions. The component cost modules were considered and their relative cost contributions are shown in Table 3. In addition to these, the realistic *FCR* of 7.5% was taken according to the NREL [35]. From the rotor and nacelle modules, the blades, drive train, and power electronics were assumed to vary with rated power, contributing 9.14%, 9.48%, and 8.27% of the total costs, respectively, and were taken as an input in Equation (31). The relative-*CoE*, which is the ratio of the *CoE* to the nominal value, was then applied in the analysis and the design parameters V_r and P_r were varied with relative-*CoE* to enable evaluation. Finally, these results were investigated to demonstrate whether the design parameters were at a minimum cost of energy or not.

Table 3. Component cost breakdown of wind turbine [35].

Cost Modules (-)	***Module Cost Share % ($/kW)***	***Module Elements (-)***	***Element Cost Share % ($/kW)***
Rotor Module	*14.29*	*Blade*	*9.14*
		Pitch assembly	*2.97*
		Hub assembly	*2.19*
Nacelle Module	*24.21*	*Nacelle structure*	4.86
		Drive train	9.48
		Nacelle electric	8.27
		Yaw assembly	1.60
Tower Module	*10.65*		
Balance of System	*16*		
Financial Costs	*6*		
Operation and Maintenance	*28.53*		

2.8. Iterative Processes

Based on the above relationships and conditions, the iterative process used for designing the realistic blade was implemented as follows:

To initiate the iterative process, the tip speed ratio, number of blades, and atmospheric parameters such as air density and viscosity were taken as constant values. Initial design wind speed was assumed and the chord lengths evaluated based on the ideal blade parameter values.

The blade element method was then applied, limiting the induction factors to converge to the ideal values followed by determining the force coefficients and flow angles element-wise as variables. Taking these results as input into the next step and with the design power as the constant constraint, the rotor radius and rotor speed were evaluated as variables till the previous and latest iteration results converged, achieving a maximum power coefficient. As a result, blade parameters such as the chord lengths and twist angles element-wise were updated by modifying the blade geometry. Hence, the blade key parameters, the power, and thrust coefficients were evaluated and recorded for further processes.

Lastly, the *CoE* and performance parameters *AEP* and *CF* were evaluated based on the specific wind distribution, examining if minimum cost of energy was achieved at the selected design wind speed and rated power. The above iterative processes were repeated till a minimum *CoE* was achieved at a specific wind speed and rated power for the specified wind distribution.

2.9. Numerical Performance Prediction and Validation

In this paper, Ansys-Fluent, a widely used CFD modelling software, was used for validation purposes considering the continuity and Navier–Stokes equations as governing equations of the flow around the blade. The four-equation turbulence model k-ω SST, suited for boundary layer and far-field flow modelling, and Reynolds-averaged form of the continuity and momentum equations were used for solving the flow around the blade.

The computational domain was modelled using a single blade in the 120° radial stream tube domain segment, with periodic faces as boundary conditions to reduce computation time. The solution was then extrapolated to other two blades to realize the results for the three-blade rotor. Hence, the cylindrical computational domain was considered with the inlet located at the upstream side in front of the blade at three-fold of the rotor radius with a diameter five times the diameter of the rotor. The outlet of the domain was located at ten times the radius of the rotor behind the rotor blade at the downstream side with a cylindrical boundary at seven times the radius of the rotor to avoid unfavorable boundary dependency effects by allowing wake expansion [41,42]. Moreover, proper boundary conditions were implemented with the design velocity as the inlet velocity and the atmospheric pressure of the selected site condition as the outlet pressure. In the computational domain, a rotating frame was applied to account for the rotor speed assuming a stationary blade as a non-slip wall boundary condition.

For the simulation to converge and solve smoothly, the computational domain was meshed employing mesh control selections. Hence, using the global mesh control, the computational domain was meshed with unstructured mesh using tetrahedral cells, which are easier to mesh complex geometry and achieve mesh quality. An advanced size function was then applied to better represent the curves, setting it to proximity and curvature at a fine relevance center. Using the local mesh control, match control and face sizing were then applied to the periodic faces and to the surface of the blade, respectively, with element size of 2mm. Moreover, prismatic type inflation layers were implemented to the blade surface at a reasonable growth rate to better represent the boundary layer flow. The wall distance y+ was limited to less than one for improved resolution of the flow in the boundary layers [41]. The wall distance y+ is a non-dimensional distance from the wall to the first mesh node and is used to describe the height of the first grid element next to a wall in the simulation. Moreover, a sphere of influence was employed at the computational domain around the blade geometry. These would improve the quality of mesh and enhance the convergence of the solution. Hence, skewness, which is most recommended for CFD, was implemented to control the quality of mesh in the simulation, confirming most of the cells to be at lower values with 0.9 as a limiting value.

Incompressible settings, at the specified design conditions, were applied to the air around the rotating blade. Incompressible RANS (Reynolds-averaged Navier–Stokes) equations were solved using a steady-state, pressure-based coupled algorithm with double precision applying pseudo transient and high-order term relaxation. Moreover, a turbulent intensity value of 5%, which is sufficient for nominal turbulence through a circular inlet, and a turbulent viscosity value of 10, which is a typically good value for external flows, were used in the simulation. The convergence of the solution was also assured, limiting the residual values for continuity, the velocities, turbulent kinetic energy, and the specific dissipation rate to less than 10^{-6}, and restricting net mass imbalances in the inlets and outlets values to less than 0.1% [42–44]. Finally, torques and forces induced by the blade profile were recorded and used for comparison with the BEM results.

On the other hand, Ashes software (simis.io), which is an analysis software for wind turbines, was used as an off-design performance prediction tool. Parameters including twist angle, chord, pitch axis, and airfoils, at their corresponding radial positions, were provided to Ashes in a table format to predict the performance of the designed blade in different conditions. The shape files for the selected airfoils, including the interpolated ones between the nominated positions, were also included. Ashes internally implements xfoil to determine the lift and drag coefficients of the provided shape files if not provided. Thus, executing it for different wind speeds, the results of TSR, C_p, and C_t were taken in table format to evaluate different characteristic curves and for further investigation. The effect of pitch angle on the performance of the blade was examined using the performance curves at various pitch angles. The best pitch angle was then selected and used to evaluate the performance results and further modify the blade geometry.

3. Results and Discussion

3.1. Element Forces and Parameters

The sectional or element induction factors and flow or twist angles found are shown in Figure 6. The values of the induction factors were close to the theoretical value in most sections except at around the root, which was due to the modifications in chord length and twist angles, as shown in Figure 6a. Around the blade root up to r/R = 0.4, the axial induction factor "a" was much lower than the theoretical value ($a = 1/3$), while the tangential induction factor a' was higher than its theoretical value ($a' = 0$). Beyond r/R = 0.4, both induction factors were close to the theoretical values, as expected. Figure 6b shows the results of the twist angle and flow angle. The twist angle had a smooth transition to zero around the root facilitating proper connection with the hub plate. The difference between the flow and twist angles shown in Figure 6b revealed the angle of attack. The angle of attack was constant (at airfoil optimum value) from the tip towards the root and significantly increased around the root due to the twist modifications implemented and the transition into the rectangular section.

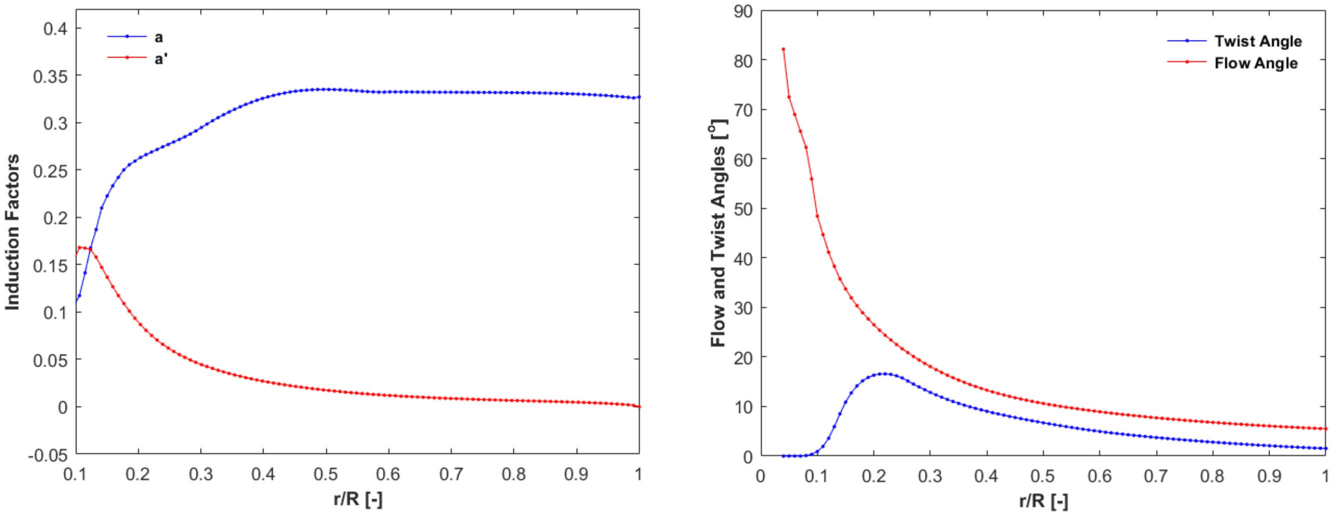

(**a**) (**b**)

Figure 6. Element induction factors and angles along the normalized blade radius at a wind speed of 10 m/s. (**a**) Induction factors vs. normalized radius. (**b**) Twist/flow angles vs. normalized radius.

Likewise, the results of the element forces dT and dQ were as shown in Figure 7. More thrust force contributions were from around the tip sections, as shown in Figure 7a, while the rotating torque was almost constant except at around the root and tip parts. The thrust force increased linearly from the root section until reaching a peak value of approximately r/R = 0.9 and decreased due to the tip losses. The span-wise power contribution of the designed blade was also as shown in Figure 7b, with the span-wise highest power contribution near the tip region at approximately r/R = 0.9, which decreased almost linearly towards the root.

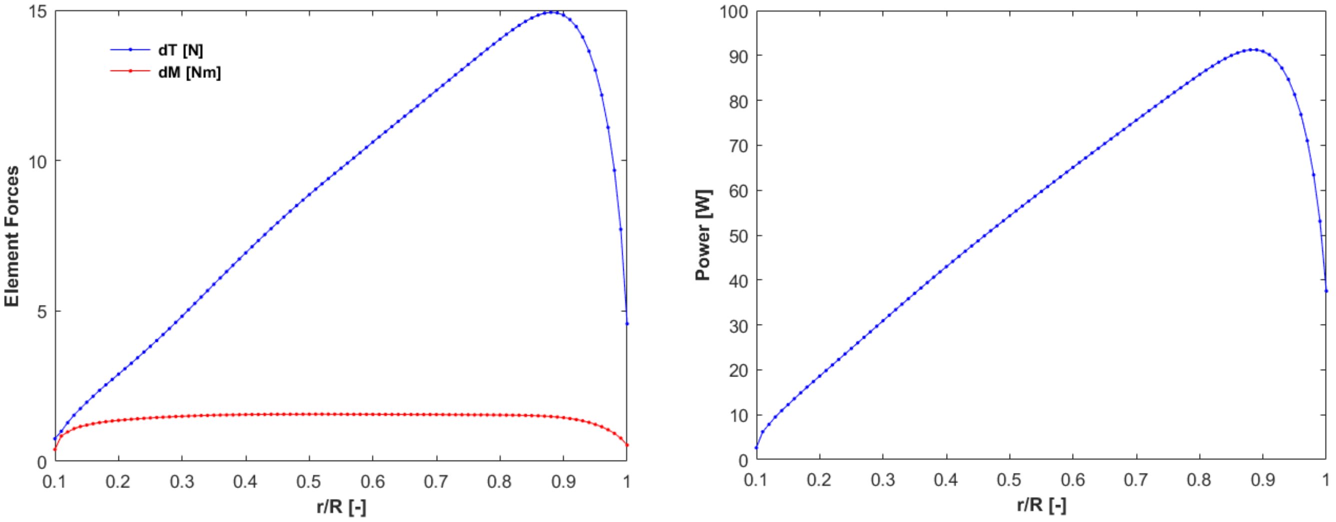

(**a**) (**b**)

Figure 7. Element forces and power along the normalized radius of the designed blade at a wind speed of 10 m/s. (**a**) Element thrust and torque vs. normalized radius. (**b**) Element power vs. normalized radius.

Finally, the blade designed based on the BEM implementation with corrected root and tip parts developed using the MATLAB code in a 3D plot, in its dimensionless form, is shown in Figure 8. The designed blade output gives an optimized radius of 2.61 m to produce 5 kW of power at 10 m/s of wind speed and the other selected design conditions.

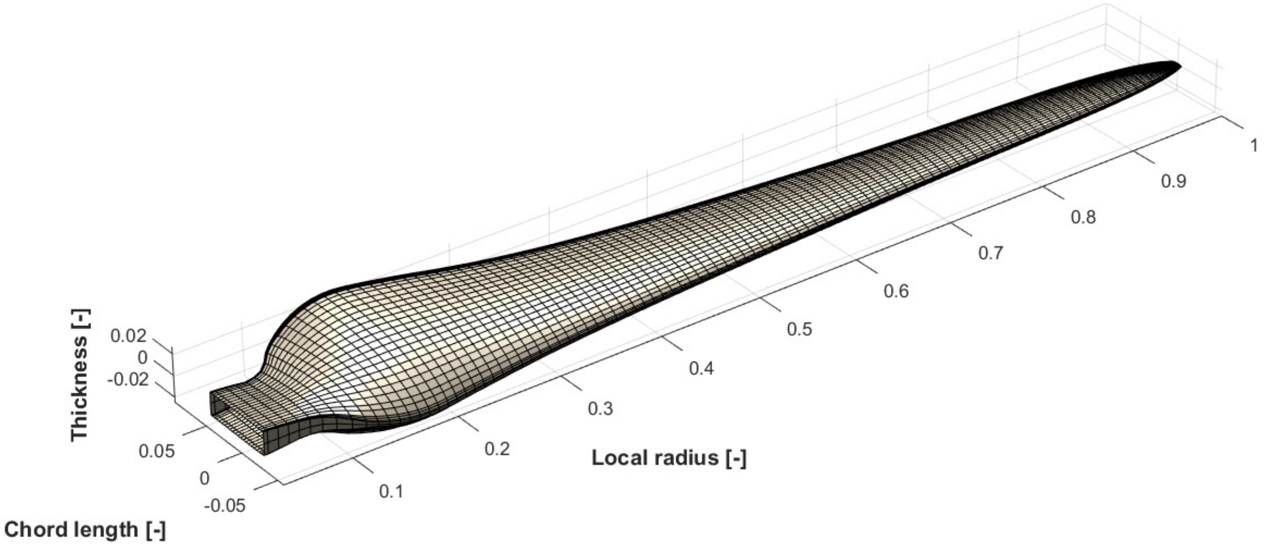

Figure 8. Three-dimensional blade geometry of the designed blade normalized with the radius.

3.2. Performance Characteristics

Different blade parameters at the design wind speed of 10 m/s, pitch angle of zero, and tip speed ratio of 7 were evaluated, with a power coefficient C_p close to 51% and thrust coefficient of approximately 82% achieved employing the MATLAB code. Corresponding torque and thrust forces of approximately 187 Nm and 807 N, respectively, were attained, as shown in Table 4. Almost the same results were gained with Ashes software, which was used to further evaluate the performance parameters at the design conditions. Ansys-Fluent simulation was used to validate the performance characteristics at the design wind speed of 10 m/s and different tip speed ratios. The results of BEM and Ansys-Fluent were in good agreement and are also shown in Table 4.

Table 4. Performance results of the designed blade at design conditions.

Parameters	*MATLAB Results*	*Ashes Results*	*Ansys Results*	*Max C_p Results*
C_p(%)	50.7	50.46	50.35	51.74
C_t(%)	81.9	81	81.64	89.9
Torque, q (nm)	186.6	186.5	184.83	159.8
Thrust force, t (n)	807.3	802.8	804.45	890.9
Optimized radius, r (m)	2.61	2.61	2.61	2.61
Rotor speed, ´Ω *(rpm)*	256	256	256	306.3
Tip speed ratio, Λ *(-)*	7	7	7	8.4

The power coefficient and torque versus tip speed ratio curves using BEM and Ansys-Fluent for a range of tip speed ratios at zero pitch angle are shown in Figure 9a,b. The C_p values were close to 50% in the tip speed ratio range of 6.5–10 and would be the preferred operating range for the designed wind turbine. It can be noted that this was not a narrow range, implying that there was a wide operation range of the blade in terms of rotor speed and wind speed with maximum C_p values. In this range, the Ansys-Fluent results agreed very well with the BEM results, and out of this range, slight deviation between the CFD and BEM results are observed. The difference could be due to the effects associated with increased angles of attack at low and high *TSR* values. Keeping the wind speed at a constant value, increasing the tip speed ratio will increase the power coefficient unless stall condition is reached. Therefore, using both BEM and Ansys-Fluent, a maximum C_p value of 51.74% was attained at a tip speed ratio of 8.4 and wind speed of 10 m/s, with a corresponding rotor speed of approximately 306 revs/min. Accordingly, in comparison to the values in most of the literature, an enhanced power coefficient was attained, signifying that implementation of the combination of the selected design processes would lead to improved performances of small wind turbines.

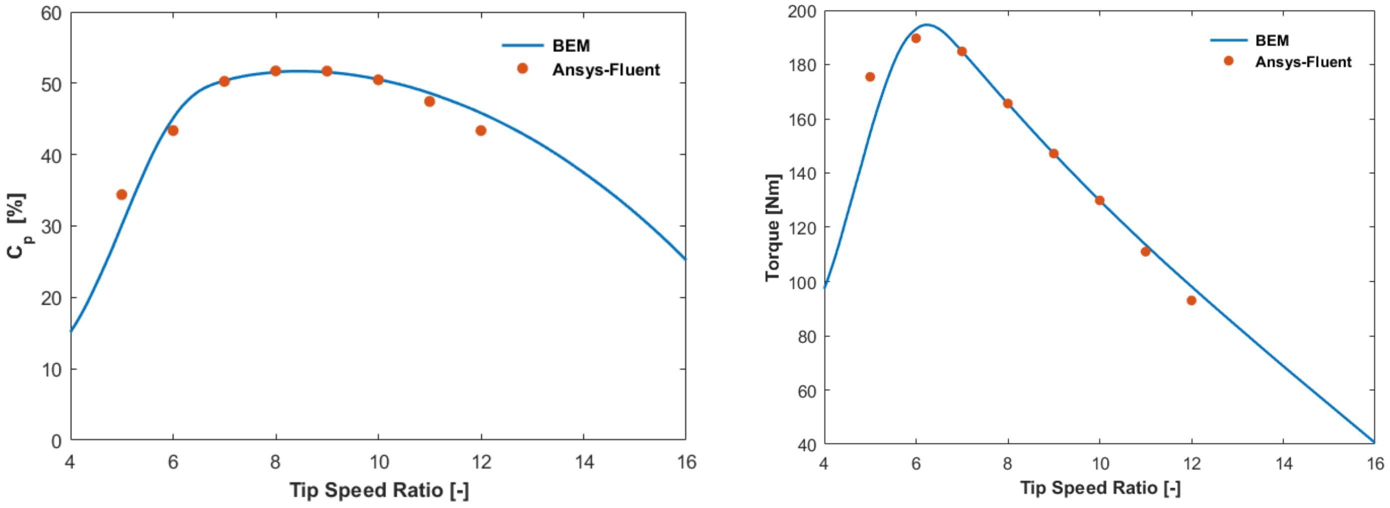

(**a**) (**b**)

Figure 9. Performance coefficient results at a wind speed of 10 m/s using BEM and Ansys-Fluent simulation. (**a**) Power coefficient vs. tip speed ratio. (**b**) Torque vs. tip speed ratio.

Results of the CFD analysis of the blade shown in Figure 10 illustrated that the pressure distribution was found to be highest on the pressure side along the leading edge. Similarly, low pressure was observed on the suction side along the leading edge, while the lowest pressure was observed towards the tip of the blade. Hence, the differences in surface pressure between the upper and lower surface of the blade create the driving torque, with higher contributions around the tip region and decreases while moving towards the root part, resulting in minimal pressure differences. Furthermore, the flow velocity patterns at five cross-sections superposed to the blade from the root to the tip are shown in Figure 11. At the root section, the velocity streamlines indicate that halfway to the chord of the blade flow separation is observed. This was expected due to the rectangular section used around the root of the blade. However, a fully attached flow with no separation was observed in the other four sections along the length of the blade. This result confirmed that there was no stall condition at the rated wind speed.

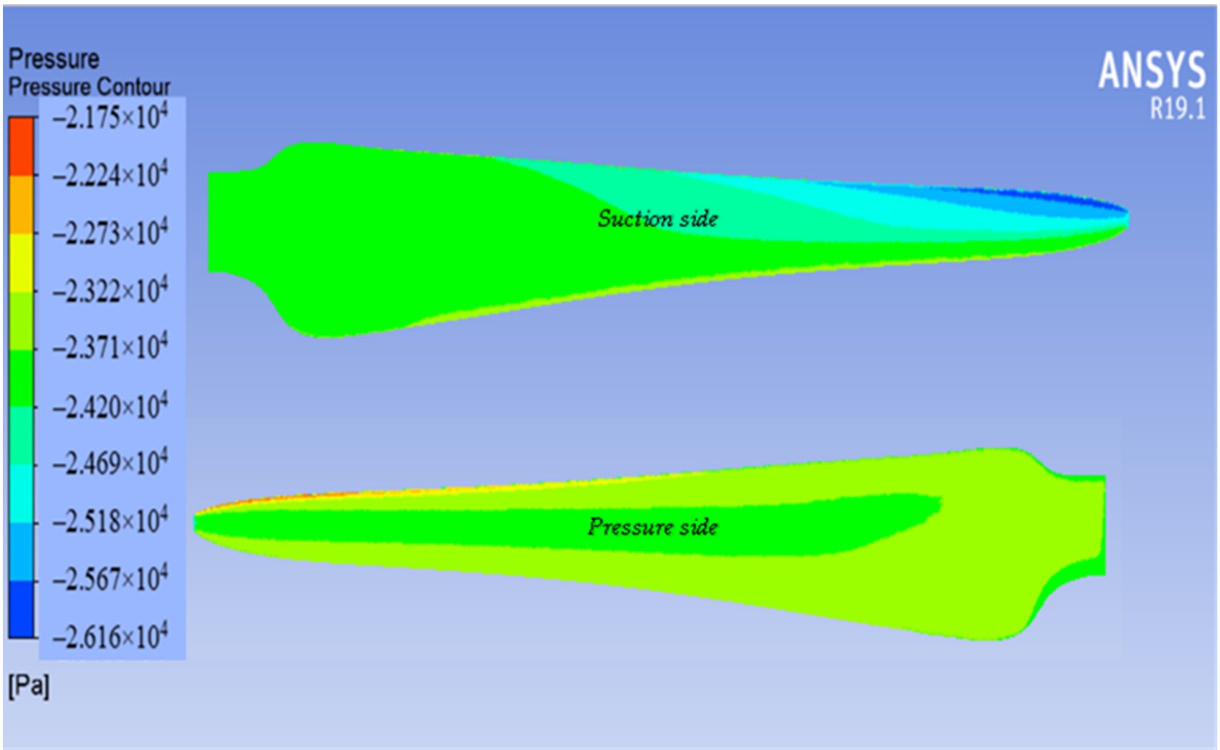

Figure 10. Pressure contour at design conditions of the blade surface for the suction and pressure sides.

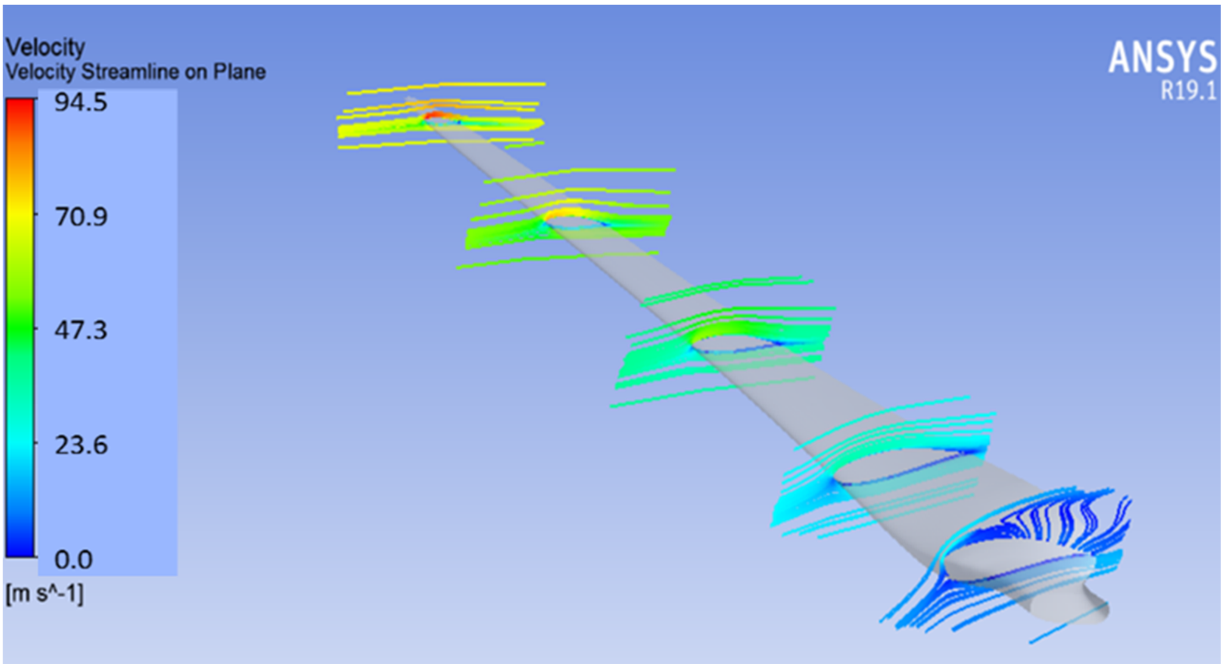

Figure 11. Velocity streamlines at design conditions of the blade surface for different radial positions.

It is essential to look into different characteristic indicator plots, for a range of tip speed ratio and rotational speed ω of the rotor, to check the features of the designed blade. Figure 12 shows the power coefficient and thrust coefficient versus *TSR* for various wind speeds. As per the power coefficient versus *TSR* and wind speed plot in Figure 12a, almost the same C_p values were shown up to *TSR* of approximately 6 for all wind speeds. At *TSR* = 5, the C_p value was approximately 30% for all wind speeds (indicated with the same color). Beyond *TSR* = 6, variation of the value of C_p with wind speed was observed reaching a maximum value at the rated wind speed of 10 m/s. At *TSR* = 8, the value of C_p was approximately 45% for low wind speeds and increased to a maximum of just above 50% at 10 m/s. Similar behavior was also observed for the thrust coefficient, as shown in Figure 12b.

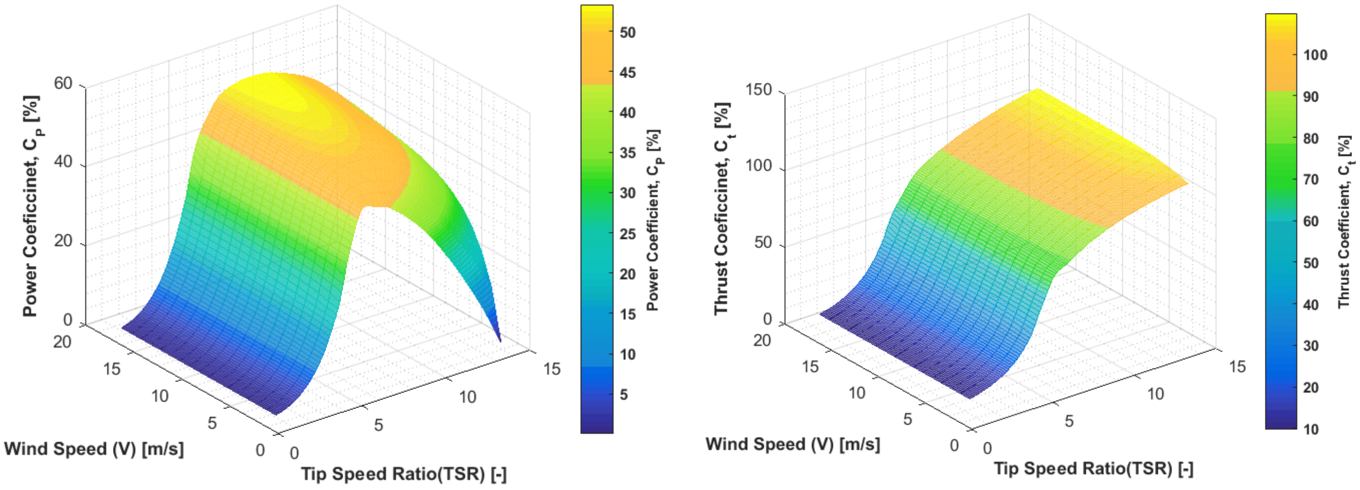

(**a**) (**b**)

Figure 12. Performance coefficients for different design parameters. (**a**) Power coefficient vs. *TSR* and wind speed, (**b**) Thrust coefficient vs. *TSR* and wind speed.

Similarly, Figure 13a,b shows power and torque versus the rotor speed. For all the wind speeds, the power curve offered maximum value for some rotor speeds corresponding to tip speed ratios of approximately 6.5–10. Maximum power tracking control mechanisms and variable speed generators provide maximum power output at different wind speeds. Among the power tracking control methods, constant tip speed ratio and maximum C_p are the most commonly used. Hence, Figure 13a,b shows power and torque characteristic curves, respectively, implementing a constant tip speed ratio of 7 and maximum power coefficient $C_{p\text{-}max}$ tracking points. The dotted lines shown in the illustrations represent variable speed operation beyond the rated wind speed. Beyond the rated wind speed to keep the turbine at the rated power, the rotor speed must be reduced. For a rated power of 5 kW and wind speed of 10 m/s (shown in the red curve), the dotted line indicates the rotor speed reaching approximately 306 rpm. Beyond a wind speed of 10 m/s, the variable speed control is required to reduce to a rotor speed of approximately 220 rpm to keep the power at 5 kW. Such methods enable small wind turbines to operate at maximum possible efficiency. Figure 13b reveals that the maximum power coefficient tracing points were away from the maximum torque points; this would minimize the applied force to the turbine structure while obtaining the highest power coefficient at lower torque values, unlike the C_p values at *TSR* = 7.

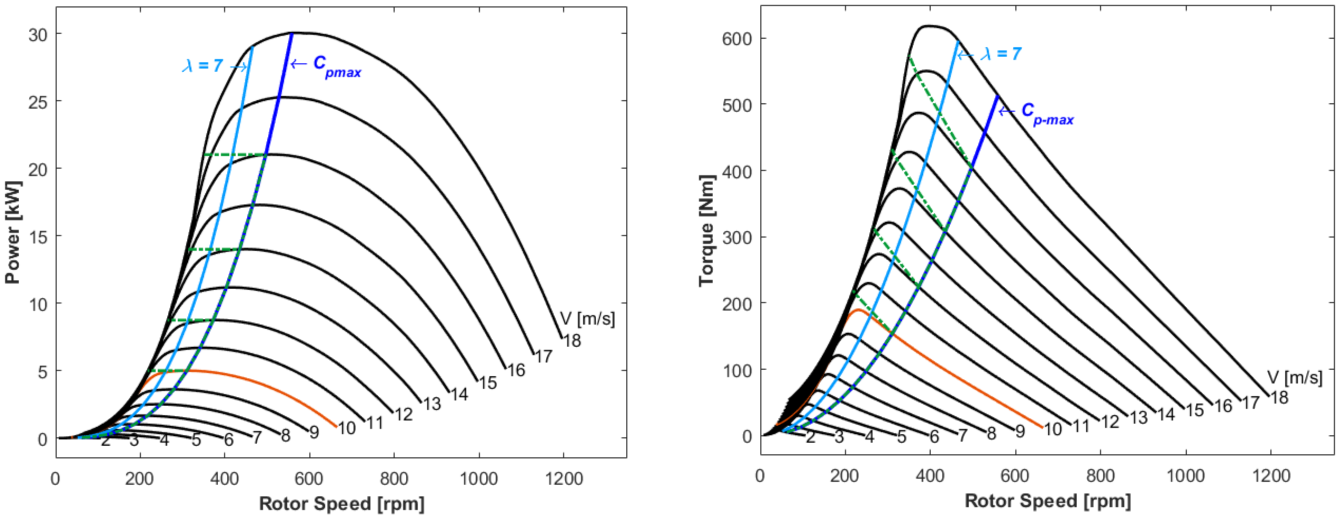

(**a**) (**b**)

Figure 13. Performance curves including variable speed operation and maximum power tracking points for the specific wind distribution. (**a**) Power vs. rotor speed. (**b**) Torque vs. rotor speed.

3.3. Effect of Pitch Angle

The effect of the pitch angle on the performance of the blade, evaluated at the design wind speed of 10 m/s, is shown in Figure 14. Positive pitch values are represented when the leading edge was twisted against the wind and negative value means the rotor was pitching to stall. Figure 14 shows the value of the power coefficient for pitch angles 0° to −5°. The power coefficient increased with a pitch angle up to −3° and then decreased for −4° and −5°. A finer three-dimensional plot of the power coefficient against the *TSR* and pitch angle is shown in Figure 15, including positive pitch values. The C_p value for a positive pitch angle demonstrated higher values at a higher *TSR* in comparison to the others. Regardless of this, the C_p at a pitch angle of −3° remains the maximum value. As a result, a maximum power coefficient of *55.37%* was found at a pitch angle of −3°, *TSR* of 8.1, and rotational speed of 295.5 rpm. Comparing the results with no pitch, it led to an increased percentage change in the power coefficient of 6.78%. Hence, a pitch angle of −3° was taken as the optimal value to adjust the twist angle to boost the blade's performance.

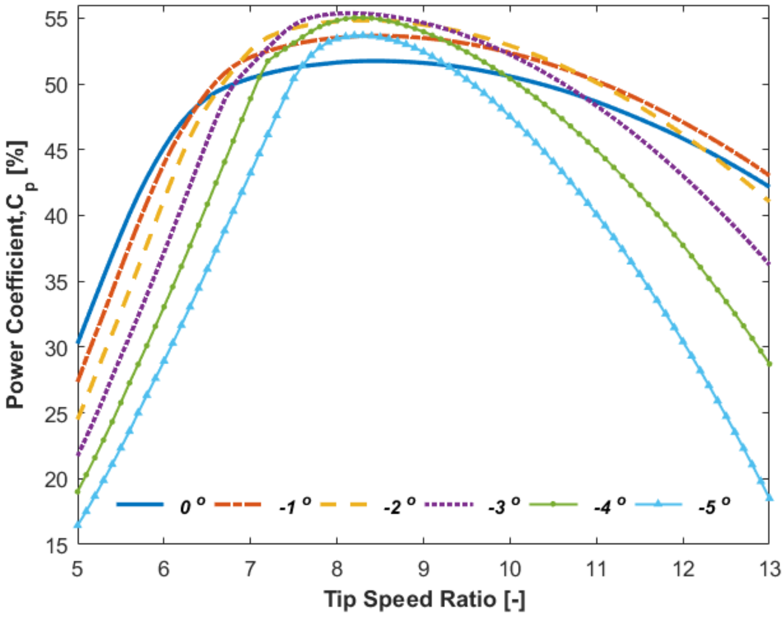

Figure 14. Power coefficient against tip speed ratio for different pitch angles at design conditions.

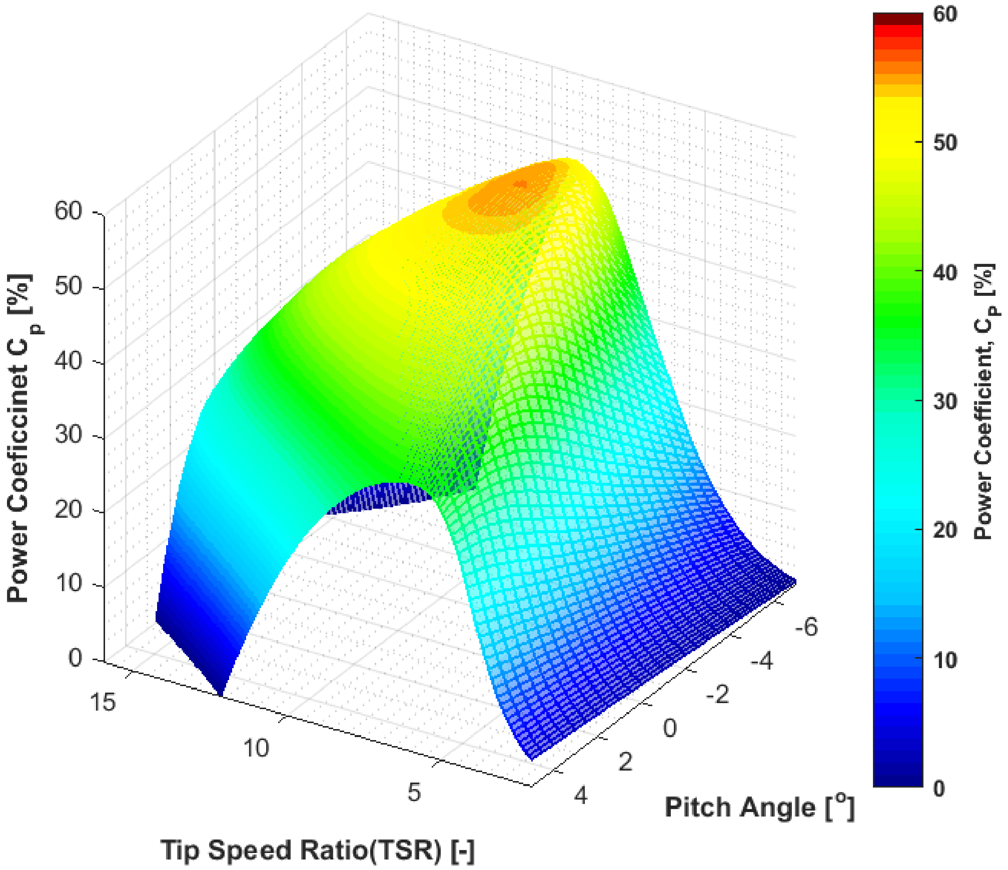

Figure 15. Power coefficient against tip speed ratio and pitch angles at design conditions.

3.4. Relative Cost of Energy

The power performance curve determined from the C_p values at the optimum pitch angle of −3° for a rated power of 5 kW and wind speed of 10 m/s is shown in Figure 16. The C_p curve and rotor speed variation are also included in Figure 16. As previously indicated in Figure 13a, rotor speed increases with wind speed until the rated condition is met and is then reduced to keep the power constant. Similar power curves could be found if the blade was to employed for different values of rated power. *AEP* and *CF* can then be calculated as a function of the rated power based on the respective power curve shown in Figure 16 and the site wind conditions, as described previously in Figure 2. *AEP* and *CF* as a function of the rated power are shown in Figure 17. *AEP* increased with rated power and became constant at high-rated power. On the other hand, *CF* decreased at a high rate with an increase in rated power. At a rated wind speed of 10 m/s and rated power of 5 kW, *AEP* of 16.98 MWh and *CF* of 38.76% were found at zero pitch angle, while *AEP* of 17.89 MWh and *CF* of 40.81% were achieved at a pitch angle of −3°. Increases in *AEP* and *CF* of 5.28% and 5.15%, respectively, were obtained at a pitch angle of −3°.

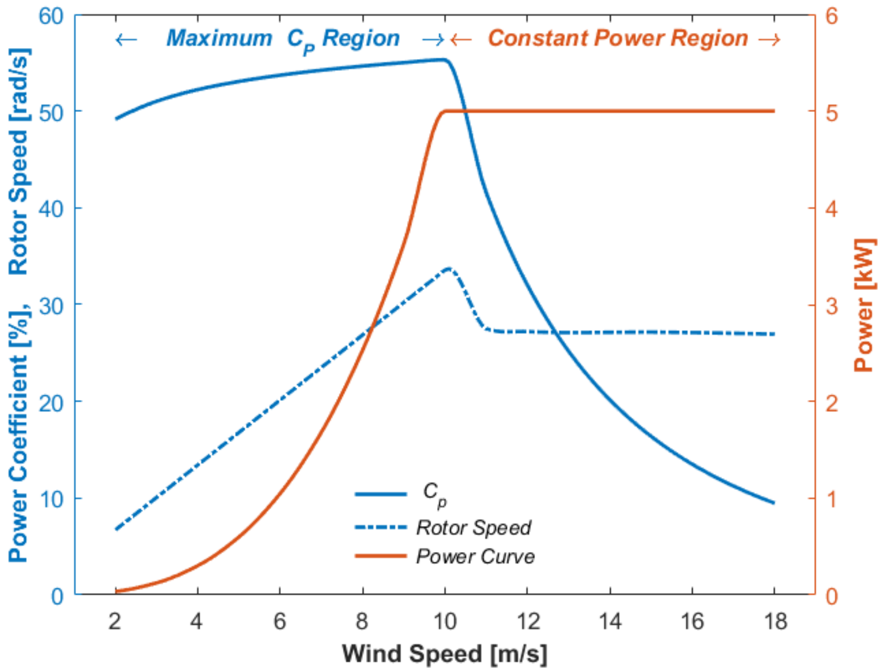

Figure 16. Power coefficient, power, and rotor speed against operating wind speed at a pitch angle of −3° generated applying variable speed operations and maximum power tracking principles.

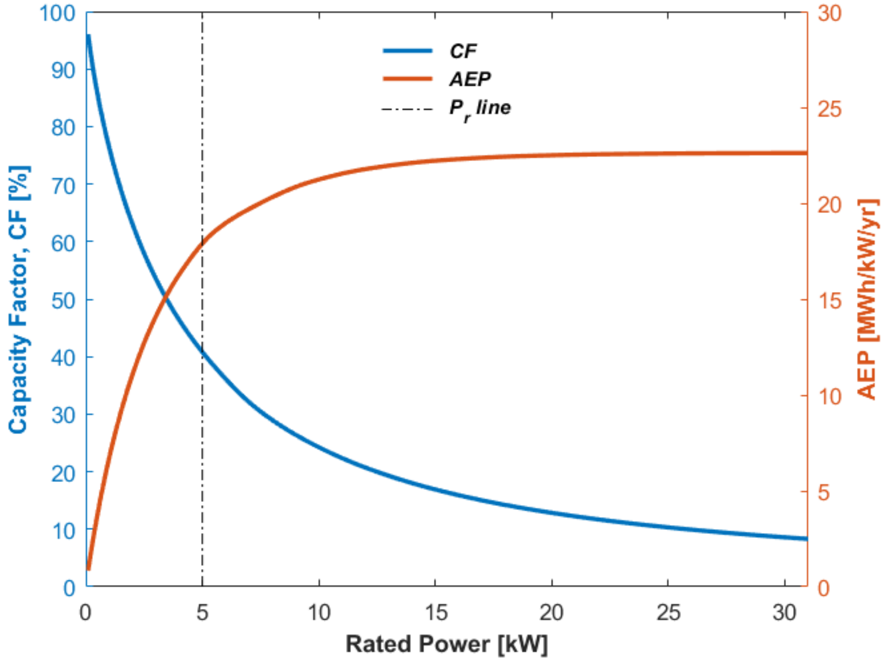

Figure 17. Annual energy production and capacity factor against rated power at −3° pitch angle.

The relative-*CoE* was calculated based on Equation (31) and by employing the *AEP* values at the respective rated power from Figure 17. In Figure 18, the relative-*CoE* is shown as a function of rated power and wind speed. Figure 18a shows the blade being used for a direct drive system, while in Figure 18b, the same blade is used for a gear drive system. The values for the direct drive system demonstrate the lowest relative-*CoE* at the selected design parameters. Figure 18a confirms that a P_r of 5 kW and V_r of 10 m/s were at the minimum relative-*CoE* values. Running the turbine at lower-rated power (<5 kW) would increase the *CoE*. This is due to the significant reduction in *AEP* compared to the reduction in cost at lower-rated power. Operating at higher-rated power (>5 kW) would also increase the *CoE*.

The increase in cost associated with higher-rated power exceeds the gain in *AEP*. Similarly, Figure 18b shows that the P_r and V_r values corresponding to the lowest relative-*CoE* were at a rated power of 3.8 kW and rated wind speed of approximately 8.9 m/sec, indicating further iterations are required to reach the optimal values for the geared system leading to a selection of different design parameters and hence different sizing of the blade. In comparison, a 2.2% increase in relative-*CoE* shall be accommodated in case there is a need to use the designed blade with the gear drive system at the rated power of 5 kW and rated wind speed of 10 m/s.

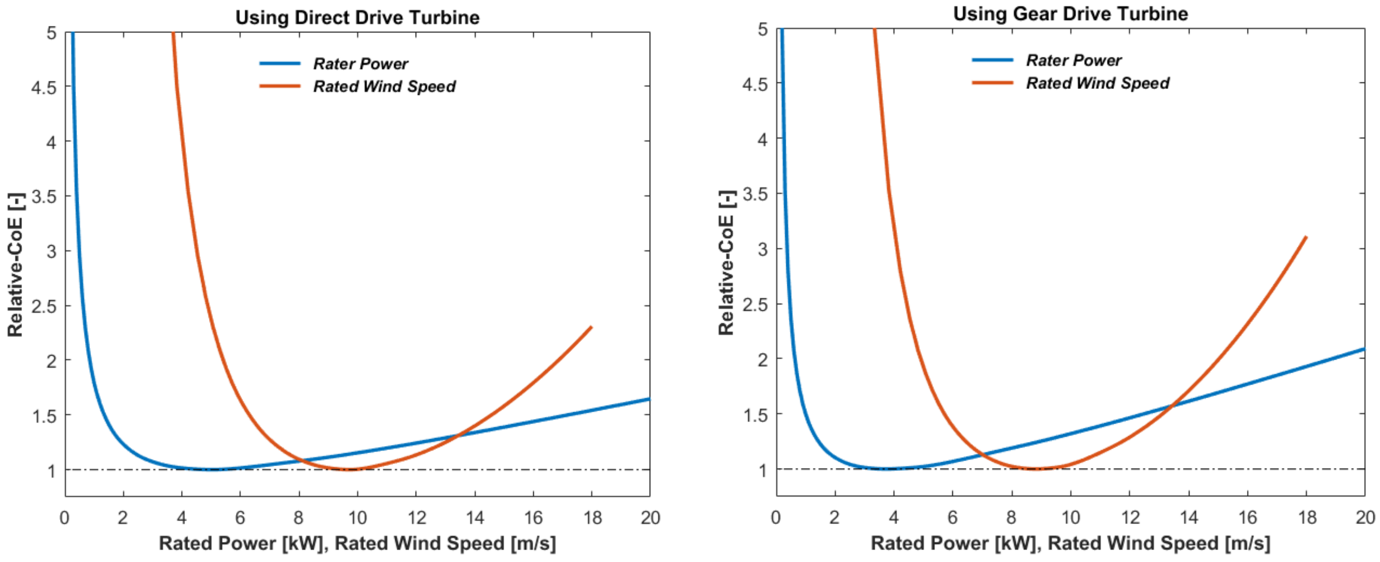

(**a**) (**b**)

Figure 18. Rated power and rated wind speed against relative-*CoE* at pitch angle of −3°. (**a**) Direct-drive system. (**b**) Gear drive system.

4. Conclusions

A typical 5 kW small wind turbine was designed with enhanced aerodynamic performance blade, applying BEM with improvements and modifications using MATLAB code and considering the cost of energy as a design parameter. The blade was made from two airfoils (S822 and S823) and their hybrids along the length and rectangular section at the root. Improvements and modifications of the BEM incorporated in the design included: tip loss factor, chord modification for a smooth blade profile employing a Bezier curve, and twist angle modification. The cost of energy, which is the ratio of the overall capital and operation cost to the *AEP*, was formulated as a function of the rated power and rated wind speed. Through iterative analysis, the optimum dimensions of the blade were found to be 2.61 m length, 40 cm maximum chord, and 30 mm maximum thickness.

The results of the BEM blade design analysis at zero pitch angle indicated that a maximum C_p value of 51.7% was attained at a tip speed ratio of 8.4, corresponding to a rotor speed of 306 rpm and wind speed of 10 m/s. The performance was further increased at an optimum pitch angle of −3° to a maximum C_p of 55.4% at a tip speed ratio of 8.1 and corresponding rotor speed of 295 rpm. The blade performance was checked employing Ashes software and modeled in Ansys software for CFD analysis. The results from both software for the power coefficient C_p and thrust coefficient C_t were found to be in good agreement with the BEM results.

Applying variable speed operation together with the maximum power tracing principles, *AEP* and *CF* values of approximately 16.98 MWh and 38.76%, respectively, were found at the rated power and wind speed with zero pitch angle. Improving the twist angle using the optimal pitch angle of −3°, *AEP* and *CF* were improved to 17.89 MWh and 40.81%, with corresponding percentage increments of 5.28% and 5.15%, respectively. Therefore, considering the cost of energy as a design parameter, enhanced performance at a lower cost of energy was achieved, and evaluating it against varying rated power, a lower relative-*CoE* was attained at the rated values for a direct drive application. In conclusion, the design and analysis procedures and modifications have demonstrated that enhanced aerodynamic performance and hence increased energy harnessing ca-pability of small wind turbines could be achieved.

Author Contributions: Conceptualization, H.K.K., L.F., M.B.K. and T.K.N.; Data curation, H.K.K.; Formal analysis, H.K.K.; Funding Acquisition, M.B.K. and T.K.N.; Investigation, H.K.K.; Methodology, H.K.K.; Project administration, M.B.K.; Resources, H.K.K., L.F., M.B.K. and T.K.N.; Software, H.K.K. and L.F.; Supervision, T.K.N., L.F. and M.B.K.; Validation, H.K.K.; Visualization, H.K.K.; Writing—original draft preparation, H.K.K.; Writing—review and editing, H.K.K., M.B.K. and T.K.N. All authors have read and agreed to the published version of the manuscript.

Funding: This research was funded by Capacity 5 project coordinated by EiT-M, Mekelle University, a collaborative project under the EnPe program of the Norwegian Government, project number (EiTM/EF/01/2007).

Conflicts of Interest: The authors declare no conflict of interest.

References

1. ICC-SWCC Directory of Certified Turbines. Available online: https://smallwindcertification.org/certified-turbines/ (accessed on 10 October 2022).
2. Global Small wind Market 2020 by Manufacturers, Regions, Type and Application, Forecast to 2025. Available online: https://www.globalinforesearch.com/ (accessed on 20 October 2020).
3. Hirahara, H.; Hossain, M.Z.; Nonomura, Y. Testing basic performance of a very small wind turbine designed for multi-purposes. *Renew. Energy* **2005**, *30*, 1279–1297. [CrossRef]
4. Karthikeyan, N.; Murugavel, K.K.; Kumar, S.A.; Rajakumar, S. Review of aerodynamic developments on small horizontal axis wind turbine blade. *Renew. Sustain. Energy Rev.* **2015**, *42*, 801–822. [CrossRef]
5. Wind Power as an Alternative to Coal. Available online: https://www.gem.wiki/Wind_power_as_an_alternative_to_coal (accessed on 20 October 2020).
6. Milivojevic, N.; Stamenkovic, I.; Schofield, N. Power and Energy Analysis of Commercial Small Wind Turbine System. In Proceedings of the 2010 IEEE International Conference on Industrial Technology, Vina del Mar, Chile, 14–17 March 2010; pp. 1739–1744.
7. Fasel, H.F.; Gross, A. *Numerical Investigation of Different Wind Turbine Airfoils*; The University of Arizona FL: Tucson, OR, USA, 2011.
8. Giguere, P.; Selig, M.S. Low Reynolds number airfoils for small horizontal axis wind turbines. *Wind Eng.* **1997**, *21*, 367–380.
9. Selig, M.S.; McGranahan, B.D. *Wind Tunnel Aerodynamic Tests of Six Airfoils for Use on Small Wind Turbines*; The University of Illinois at Urbana-Champaign: Champaign, IL, USA, 2004.
10. Tangler, J.L.; Somers, D.M. *NREL Airfoil Families for HAWTs*; National Renewable Energy Laboratory: Golden, CO, USA, 1995.
11. Tangler, W.; Van Rooij, R. Summary of the Delft University wind turbine dedicated airfoils. *J. Sol. Energy Eng. ASME* **2003**, *125*, 488–496.
12. Giguere, P.; Selig, M.S. Aerodynamic effects of leading-edge tape on airfoils at low Reynolds numbers. *Wind Eng.* **1999**, *2*, 125–136. [CrossRef]
13. Manwell, J.F.; McGowan, J.G.; Rogers, A.L. *Wind Energy Explained: Theory, Design and Application*; John Wiley & Sons Ltd.: Chichester, UK, 2002.
14. Burton, T.; Jenkins, N.; Sharpe, D.; Bossanyi, E. *Wind Energy Hand Book*; John Wiley & Sons Ltd. Publication: Chichester, UK, 2011.
15. Mojtaba, T.; Ghazale, K.; Mehran, M.; Mojtaba, M. Aerodynamic design of horizontal axis wind turbine with innovative local linearization of chord and twist distributions. *Energy* **2017**, *131*, 78–91.
16. Frøyd, L.; Ole, G.D. A Conceptual Design Method for Parametric Study of Blades for Offshore Wind Turbines. In Proceedings of the ASME 30th International Conference, Rotterdam, The Netherlands, 21–26 May 2011.
17. Prandtl, L.; Betz, A. Vier Abhandlungen zur Hydrodynamik und Aerodynamik. *Göttinger Nachr. Göttingen* **1927**, *3*, 88–92.
18. Glauert, H. *Windmills and Fans-Aerodynamic Theory*; Julius Springer: Berlin, Germany, 1935.
19. Shen, W.Z.; Mikkelsen, R.; Sørensen, J.N. Tip Loss Corrections for Wind Turbine Computations. *Wind. Energy* **2005**, *8*, 457–475. [CrossRef]
20. Sun, Z.; Chen, J.; Shen, W.Z.; Zhu, W.J. Improved blade element momentum theory for wind turbine aerodynamic computations. *Renew. Energy* **2016**, *96*, 824–831. [CrossRef]
21. Hau, E. *Wind Turbines: Fundamentals, Technologies, Application, Economics*, 2nd ed.; Springer Science & Business Media: Berlin, Germany, 2006.

22. *IEC 61400-2*; Wind turbines. Part 2: Design Requirements for Small Wind Turbines. International Electro-Technical Commission: Geneva, Switzerland, 2006.
23. Jamieson, P. *Innovation in Wind Turbine Design*; John Wiley & Sons Ltd.: Chichester, UK, 2011.
24. Bak, C. *Aerodynamics Design of Wind Turbine Rotors*; Brøndsted, P., Rogier, P.L., Nijssen, Eds.; Advances in wind turbine blade design and materials; Woodhead Publishing Limited: Cambridge, UK, 2013; pp. 59–107.
25. Bianchi, F.D.; De Battista, H.; Mantz, R.J. *Wind Turbine Control Systems: Principles, Modeling, and Gain Scheduling Design*; Springer: London, UK, 2007.
26. Madsen, H.A.; Bak, C.; Døssing, M.; Mikkelsen, R.; Øye, S. Validation and modification of the Blade Element Momentum theory based on comparisons with actuator disc simulations. *Wind. Energy* **2010**, *13*, 373–389. [CrossRef]
27. Døssing, M.; Madsen, H.A.; Bak, C. Aerodynamic optimization of wind turbine rotors using a blade element momentum method with corrections for wake rotation and expansion. *Wind. Energy* **2012**, *15*, 563–574. [CrossRef]
28. Bai, C.J.; Wang, W.C. Review of computational and experimental approaches to the analysis of aerodynamic performance in horizontal-axis wind turbines (HAWTs). *Renew. Sustain. Energy Rev.* **2016**, *63*, 506–519. [CrossRef]
29. Moshfeghi, M.; Song, Y.J.; Xie, Y.H. Effects of near-wall grid spacing on SST-K–ω model using NREL Phase VI horizontal axis wind turbine. *J. Wind. Eng. Ind. Aerodyn.* **2012**, *107–108*, 94–105. [CrossRef]
30. Sørensen, N.N.; Bechmann, A.; Réthoré, P.E.; Zahle, F. Near wake Reynolds-averaged Navier–Stokes predictions of the wake behind the MEXICO rotor in axial and yawed flow conditions. *Wind. Energy* **2014**, *17*, 75–86. [CrossRef]
31. Richie, G.; Zhiwei, G. Pitch control for wind turbine systems using optimization, estimation and compensation. *Renew. Energy* **2016**, *91*, 501–515.
32. Papi, F.; Nocentini, A.; Ferrara, G.; Bianchini, A. On the Use of Modern Engineering Codes for Designing a Small Wind Turbine: An Annotated Case Study. *Energies* **2021**, *14*, 1013. [CrossRef]
33. Sudhamshu, A.R.; Pandey, M.C.; Sunil, N.; Satish, N.S.; Mugundhan, V.; Velamati, R.K. Numerical study of effect of pitch angle on performance characteristics of a HAW. *Eng. Sci. Technol. Int.* **2016**, *19*, 632–641.
34. Rocha, P.A.C.; Araujo, J.W.C.; Lima, R.J.P.; Silva, M.E.V.; Albiero, D.; Andrade, C.F.; Carneiro, F.O.M. The effects of blade pitch angle on the performance of small-scale wind turbine in urban environments. *Energy* **2018**, *148*, 169–178. [CrossRef]
35. Stehly, T.; Philipp, B. *2018 Cost of Wind Energy Review*; National Renewable Energy Laboratory: Golden, CO, USA, 2020; NREL/TP-5000-74598.
36. International Renewable Energy Agency. *Renewable Energy Technologies: Cost Analysis of Wind Power*; IRENA: ABU Dhabi, United Arab Emirates, 2012.
37. Perkin, S.; Garrett, D.; Jensson, P. Optimal Wind turbine Selection Methodology: A Case-Study for Burfell Iceland. *Renew. Energy* **2015**, *75*, 165–172. [CrossRef]
38. Andrew, N.S.; Rick, D.; Patrick, J.M. Objectives and constraints for wind turbine optimization. *J. Sol. Energy Eng.* **2014**, *136*, 0410101-12. [CrossRef]
39. Kelele, H.K.; Nielsen, T.K.; Frøyd, L.; Bayray, K.M. Catchment Based Aerodynamic Performance Analysis of Small Wind Turbine Using a Single Blade Concept for a Low Cost of Energy. *Energies* **2020**, *13*, 5838. [CrossRef]
40. Lucas, I.A.; Oyama, D.Q.; Alex, M.A.; Augusto, A.C.; Ciro, C.R.; Eduardo, J.A.; Guilherme, J.A.; Weinio, F.A. Analysis of Weibull Parameters for Wind Power Generation. In Proceedings of the 24th ABCM International Congress of Mechanical Engineering, Curitiba, PR, Brazil, 15 February 2017.
41. Hansen, M.O.L.; Sørensen, J.N.; Voutsinas, S.; Sørensen, N.; Madsen, H.A. State of the art in wind turbine aerodynamics and aeroelasticity. *Prog. Aerosp. Sci.* **2006**, *42*, 285–330. [CrossRef]
42. Wang, L.; Quant, R.; Kolios, A. Fluid0-structure interaction modeling of horizontal-axis wind turbine blades based on CFD and FEA. *J. Wind. Eng. Ind. Aerodyn.* **2016**, *158*, 11–25. [CrossRef]
43. Choi, N.J.; Nam, S.H.; Jeong, J.H.; Kim, K.C. Numerical study on the horizontal Axis turbines arrangement in a wind farm: Effect of separation distance on the turbine aerodynamic power output. *J. Wind. Eng. Ind. Aerodyn.* **2013**, *117*, 11–17. [CrossRef]
44. Bourdin, P.; Wilson, J.D. Wind break aerodynamics: Is computational fluid dynamics reliable? *Bound. Layer Meteorol.* **2008**, *126*, 181–208. [CrossRef]